Sequential Characterization of Atrial Tachyarrhythmias Based on ECG Time-Frequency Analysis

Martin Stridh*, *Member, IEEE*, Leif Sörnmo, *Member, IEEE*, Carl J. Meurling, and S. Bertil Olsson

***Abstract*—A new method for characterization of atrial arrhythmias is presented which is based on the time-frequency distribution of an atrial electrocardiographic signal. A set of parameters are derived which describe fundamental frequency, amplitude, shape, and signal-to-noise ratio. The method uses frequency-shifting of an adaptively updated spectral profile, representing the shape of the atrial waveforms, in order to match each new spectrum of the distribution. The method tracks how well the spectral profile fits each spectrum as well as if a valid atrial signal is present. The results are based on the analysis of a learning database with signals from 40 subjects, of which 24 have atrial arrhythmias, and an evaluation database with 211 patients diagnosed with atrial fibrillation. It is shown that the method robustly estimates fibrillation frequency and amplitude and produces spectral profiles with narrower peaks and more discernible harmonics when compared to the conventional power spectrum. The results suggest that a rather strong correlation exist between atrial fibrillation frequency and f wave shape. The developed set of parameters may be used as a basis for automated classification of different atrial rhythms.**

***Index Terms*—Atrial fibrillation, ECG, shape characterization, time-frequency analysis.**

I. Introduction

ATRIAL fibrillation is the most common sustained arrhythmia and affects as many as 5%–6% of those with age over 65 [1]–[3]. The most widely accepted hypothesis explaining the mechanisms behind the perpetuation of atrial fibrillation was presented already in the 60s, and suggests that multiple wandering wavefronts propagate throughout the atria causing so-called reentry loops [4]–[6]. Larger and fewer wavefronts result in lower local activation frequencies, and vice versa [7]. The minimum size of an activation wavefront of a reentry loop depends on atrial refractoriness and conduction velocity. Several invasive studies have demonstrated that the refractory period of the fibrillating atria can be assessed from measurements on local cycle length assuming a constant conduction velocity [8], [9]. In mapping studies, the number of simultaneous activation wavefronts has been used to describe organization of the arrhythmia: a high degree of organization reflects few wavelets circulating in the atria whereas a low degree reflects several wavelets [6], [10]. It has been established that a rather strong correlation exists between organization and local fibrillation frequency [10]. In addition to local fibrillation frequency as a measure of organization, other measures representing the number of wavefronts have been suggested [11]. The significance of atrial refractoriness has been the subject of considerable recent research efforts. It has been shown that atrial fibrillation itself causes shortening of the refractory period by which it practically can sustain itself—a phenomenon referred to as "electrical remodeling" [12]–[14]. However, the exact mechanisms behind atrial fibrillation remain uncertain.

Noninvasive analysis of atrial fibrillation has evolved from being based on rather simple measures reflecting f wave amplitude in the electrocardiogram (ECG) [15], [16], to more detailed characterization based on power spectral techniques [17], [18]; such techniques were later improved and further validated [19], [20]. The main quantity of interest in power spectral analysis is the location of the dominant peak, conveying information on the dominant atrial fibrillation frequency. This quantity has in both invasive and intraoperative studies been found to be proportional to the refractory period. The same observation applies to noninvasive measurements, as confirmed by intraatrial recordings [6], [10], [21].

Spectral analysis requires that the ventricular activity in the surface ECG is cancelled by signal processing techniques such that an atrial signal is derived—the residual ECG. Separation of the two activities has been accomplished by subtraction of an averaged QRST complex from each of the individual complexes [20], [22], [23]. However, average beat subtraction is associated with poor performance in cases of morphologic beat-to-beat changes such that the residual ECG still contains remains of ventricular activity. As a consequence, novel approaches have been developed for improving the separation of atrial and ventricular activity based on spatiotemporal optimization techniques [24], [25], principal component analysis [26], blind source separation [27], artificial neural networks [28], and separate QRS complex and T wave template subtraction [29]. The performance of the first three approaches were compared in a recent study [30].

From an electrophysiological viewpoint there are reasons to believe that the fibrillatory waveforms, as measured on the body surface, have time-dependent properties since they reflect complex patterns of electrical activation wavefronts. Information inferred from the power spectrum reflects the *average* signal behavior observed over a long time interval, usually several min-

Manuscript received December 16, 2002; revised May 11, 2003. This work was supported by a grant from the Swedish Research Council. *Asterisk indicates corresponding author.*

*M. Stridh is with the Department of Electroscience, Lund University, SE-221 00 Lund, Sweden (e-mail: msh@es.lth.se).

L. Sörnmo is with the Department of Electroscience, Lund University, SE-221 00 Lund, Sweden.

C. J. Meurling and S. B. Olsson are with the Department of Cardiology, Lund University, SE-221 00 Lund, Sweden..

Digital Object Identifier 10.1109/TBME.2003.820331

utes. Hence, it is not obvious whether a broad spectral peak reflects a multi-component signal or a temporal variation in frequency of a single component. Although power spectral analysis may have considerable clinical value, it cannot characterize short term variations of the atrial cycle length.

Recently, we suggested a new method for estimation of the atrial fibrillation frequency which, based on time-frequency analysis, provides a more detailed temporal characterization of atrial signals [31]. The strategy chosen was to analyze signals on a second-to-second basis using an iterative frequency estimation technique based on the cross Wigner Ville distribution (XWVD). In the XWVD-based method it is assumed that the atrial signal is modeled as a frequency-modulated sinusoid, i.e., only the fundamental frequency is estimated. Our method revealed considerable temporal variation of the fibrillation frequency in a majority of signals, thereby explaining the broad spectral peaks often found in the power spectrum of a 1-min record. The potential value of using a high temporal resolution was further illustrated by the following two situations: in certain patients the typical, irregular rhythm of atrial fibrillation was intermittently interrupted by short intervals of highly regular rhythms. Such intervals were found in the frequency trends produced by the XWVD-based method. The other situation was represented by changes in fibrillation frequency as caused by various types of interventions, changes which were tracked by the method.

A different strategy, not only related to the fundamental frequency, but also to the harmonic pattern of the atrial electrograms was recently presented for measuring the degree of organization of atrial activity [32]. In that strategy, a fundamental frequency with a distinct set of harmonics is considered to reflect fewer wavelets circulating in the atria. On the other hand, a larger number of wavelets results in a less "organized spectrum" without a distinct harmonic pattern.

Waveform shape is an adjunct to information on dominant fibrillation frequency and is likely to provide valuable diagnostic information. However, shape descriptors have so far not been considered in conjunction with atrial fibrillation in the ECG. Our idea is to explore shape as reflected by the time-frequency distribution of atrial fibrillation: the fibrillatory waveforms are characterized by a signal pattern whose sharpness is reflected by the number of harmonics contained in the distribution; this idea would be equally valid for the analysis of atrial flutter and tachycardia.

In this paper, a new method for characterization of atrial arrhythmias is proposed which, by using a time-frequency distribution with a logarithmic frequency scale for each new spectrum, adaptively estimates a spectral profile representing the shape of the waveforms. The spectral profile is then used to robustly estimate the local fundamental frequency and the amplitude of the atrial signal. A set of parameters are introduced which describe shape, signal-to-noise ratio (SNR) of the spectral profile, and how well the spectral profile matches each spectrum. One important goal is to perform feature extraction which can serve as a basis for automated classification of atrial arrhythmias. The suggested method is well-suited for real-time applications since the residual ECG is sequentially analyzed in blocks of 1–2 s.

The paper is organized as follows: after a brief summary of some general properties of atrial signals in Section II, the signal model and the estimation procedure are presented in Section III. A model of signal shape, which is based on the spectral profile, is then introduced in Section IV. Using the two different databases described in Section V, the performance of the proposed method is exemplified and investigated in Section VI.

II. Signal Properties

The signal properties of atrial activity in the surface ECG vary vastly between different conditions: from normal P waves during normal sinus rhythm, various types of AV block, atrial tachycardia and atrial flutter, to rapid and highly irregular f waves in atrial fibrillation. Regularly occurring signals exhibit a harmonic spectral pattern determined by the waveform shape. Therefore, regular atrial signals have a spectrum characterized by a fundamental frequency, representing the repetition rate, and one or several harmonics describing shape. Even irregular arrhythmias such as atrial fibrillation may be viewed as being essentially regular over short segments (<2 s), thereby exhibiting a harmonic spectral pattern that characterizes the f wave shape; however, the spectral peaks become less distinct when irregular arrhythmias are analyzed. In this paper, it is, therefore, hypothesized that different types of atrial signals can be characterized by fundamental frequency and a number of harmonics.

The frequency interval needed to represent an atrial signal is determined by the fundamental frequency and the highest harmonic. Since the focus of the present study is the characterization of atrial fibrillation, the frequency interval 2.5–25 Hz is considered as sufficient; this interval is also sufficient for characterization of atrial flutter and rapid tachycardias. The lower interval limit is chosen as a trade-off between the requirements of analyzing slow repetition rates and using a short time window (2–2.5 s) for sufficient time resolution. If a too long window is used, signal irregularities become too pronounced and may destroy the harmonic pattern. In addition, the spectral analysis becomes vulnerable to QRS residuals since several RR intervals may be included in the analyzed signal segment. On the other hand, a too short window implies that frequencies of about 2.5 Hz and lower cannot be accurately estimated. The main motivation for selecting the upper limit is that the highest discernible harmonic of atrial signals is below 25 Hz.

III. Signal Estimation

We propose a new method for characterization of an atrial signal which is based on its time-frequency distribution. A preprocessing stage including baseline filtering and QRST cancellation is used to produce such a signal from the ECG (Section III-A). An initial *spectral profile* $\boldsymbol{\phi}_0$ is defined such that it contains a single peak at the initial *fundamental position* p_0 and elsewhere a low amplitude, white noise floor. The initial spectral profile, which mimics a sinusoidal signal, is then gradually adapted to the repetition rate and the harmonic pattern of the prevailing signal. For each signal segment, the following four main steps are performed.

1) The spectrum $\mathbf{q}_l$ of the l^{th} segment is calculated using a nonuniform, discrete Fourier transform and appended to the time-frequency distribution (Section III-B).
2) Weighted least squares (WLS) estimation is used to jointly determine the *frequency shift* θ_l, existing between $\mathbf{q}_l$ and the spectral profile $\boldsymbol{\phi}_l$, and the *amplitude* a_l of the observed signal. The *model error* e_l is calculated once the estimates of θ_l and a_l are available (Section III-C).
3) The spectral profile $\boldsymbol{\phi}_l$ is updated with the frequency-shifted version of $\mathbf{q}_l$, and then shifted to the fundamental position p_l determined by the position of the peak contained in an exponentially averaged input spectrum $\mathbf{s}_l$ (Section III-D).
4) A set of parameters characterizing $\boldsymbol{\phi}_l$ is estimated: the *normalized peak amplitude* b_l, the *exponential decay* γ_l, and the *signal-to-noise ratio* κ_l (Section IV).

The proposed method is summarized by the block diagram in Fig. 1. The set of parameters mentioned in the above four steps, i.e., $\theta_l, a_l, e_l, b_l, \gamma_l, \kappa_l$, serves as the basis for the subsequent arrhythmia analysis. Trending of these parameters may, evidently, be combined with other types of information extracted in the ECG preprocessing stage, e.g., the series of RR intervals.

A. Preprocessing

The ECG signal is filtered for removal of baseline wander using a highpass, linear phase filter with a cut-off frequency at 0.5 Hz. Our spatiotemporal QRST cancellation technique is used to extract the atrial activity from the ECG [25]. The cancellation method, which accounts for changes in QRS morphology due to alterations in the electrical axis of the heart, has been found to perform considerably better than lead-by-lead average beat subtraction. The resulting residual ECG signal contains primarily atrial activity, e.g., P waves during sinus rhythm and f waves during atrial fibrillation. Since the spectral content of interest in the residual ECG is below 25 Hz, the signal is downsampled from 1 kHz to $f_s = 50$ Hz using proper lowpass filtering and decimation. In addition, the downsampling operation has the advantage of reducing the amount of data to be processed for time-frequency analysis.

B. Time-Frequency Analysis

The residual ECG $x(n)$ is, for the l^{th} signal segment ($l = 0, 1, \ldots$), represented by the vector

$$\mathbf{x}_l = \begin{bmatrix} x(lL) \\ \vdots \\ x(lL+N-1) \end{bmatrix} \tag{1}$$

where N denotes the segment length, and L the distance between consecutive segments. Each spectrum of the nonuniform short-term Fourier transform is calculated as

$$\mathbf{q}_l = \mathbf{F}\mathbf{W}\mathbf{x}_l \tag{2}$$

where $\mathbf{F}$ is a $K \times N$ matrix that defines a K-point, nonuniform, discrete Fourier transform matrix. The matrix $\mathbf{F}$ is based on the frequency vector $\mathbf{f} = [f_0 \ldots f_{K-1}]^T$ such that

$$\mathbf{F} = \begin{bmatrix} \mathbf{1} & e^{-j2\pi\mathbf{f}} & e^{-j2\pi\mathbf{f}2} & \ldots & e^{-j2\pi\mathbf{f}(N-1)} \end{bmatrix} \tag{3}$$

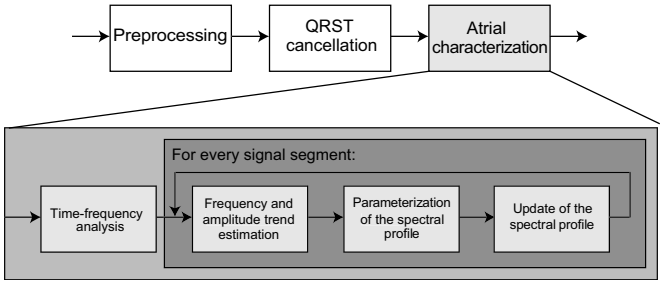

Fig. 1. Block diagram of the proposed method for time-frequency analysis of atrial signals. Each new time slice of the time-frequency distribution is aligned to the a spectral profile in order find estimates of the frequency and amplitude. The spectral profile is then parameterized and updated.

where $\mathbf{1}$ denotes a column vector of length K with all elements equal to one and j is the imaginary unit. The elements of the $N \times N$ diagonal matrix $\mathbf{W}$ define a window function. In the following, the phase of the spectrum $\mathbf{q}_l$ is ignored and, therefore, $\mathbf{q}_l$ is redefined such that

$$|\mathbf{q}_l| \rightarrow \mathbf{q}_l. \tag{4}$$

In the present method, the nonuniform short-term Fourier transform makes use of a logarithmic frequency scale

$$f_k = f_0 \cdot 10^{\frac{k}{K}}, \quad k = 0, \ldots, K-1 \tag{5}$$

because doubling in frequency for the entire spectrum corresponds to the same number of frequency bins. In this way, the harmonic patterns of two spectra with different fundamental frequencies can be matched—an important feature when estimating the frequency shift of each new spectrum that best matches the spectral profile.

C. Signal Model and Parameter Estimation

Signal Model: The atrial signal properties described in Section II offer some motivation for the following signal model: each spectrum $\breve{\mathbf{q}}_l$ is modeled as an amplitude-scaled (a_l) and frequency-shifted (θ_l) version of a known, real-valued spectral profile $(\tilde{\boldsymbol{\phi}}_l)$

$$\breve{\mathbf{q}}_l = a_l \mathbf{J}_{\theta_l} \tilde{\boldsymbol{\phi}}_l \tag{6}$$

where $\tilde{(\cdot)}$ denotes that the vector is pre- and appended with Θ points (i.e., the maximum number of frequency shifts) in order to allow that different parts of $\tilde{\boldsymbol{\phi}}_l$ can be selected. It is assumed that the peaks of the spectral profile are considerably larger than the noise floor. The 2Θ extra points have the same value as the noise floor. There are $2\Theta+1$ different sets with K samples that can be selected from $\tilde{\boldsymbol{\phi}}_l$ using the shift matrix $\mathbf{J}_{\theta_l}$

$$\mathbf{J}_{\theta_l} = \begin{bmatrix} \mathbf{0}_{K\times(\Theta+\theta_l)} & \mathbf{I}_{K\times K} & \mathbf{0}_{K\times(\Theta-\theta_l)} \end{bmatrix}, \quad -\Theta \le \theta_l \le \Theta \tag{7}$$

where the identity matrix $\mathbf{I}$ and the zero matrix $\mathbf{0}$ have dimensions as indicated by their subscripts.

Parameter Estimation: Weighted least squares estimation of θ_l and a_l is based on the cost function

$$\mathcal{J}(\theta_l, a_l) = \left(\mathbf{q}_l - a_l \mathbf{J}_{\theta_l} \tilde{\boldsymbol{\phi}}_l\right)^T \mathbf{D} \left(\mathbf{q}_l - a_l \mathbf{J}_{\theta_l} \tilde{\boldsymbol{\phi}}_l\right) \tag{8}$$

where $\mathbf{D}$ is a $K \times K$ diagonal matrix that may be designed to weight frequency components differently. Such weighting has general value when it is of interest to emphasize certain spectral

intervals. More importantly, weighting turns out to be a necessary operation in order to correct for the oversampling that occurs at lower frequencies using logarithmic frequency sampling. We begin the minimization of $\mathcal{J}(\theta_l, a_l)$ with respect to a_l and θ_l by rewriting (8) such that

$$\mathcal{J}(\theta_l, a_l) = \mathbf{q}_l^T \mathbf{D}\mathbf{q}_l - 2a_l \mathbf{q}_l \mathbf{D}\mathbf{J}_{\theta_l}\tilde{\boldsymbol{\phi}}_l + a_l^2 \left(\mathbf{J}_{\theta_l}\tilde{\boldsymbol{\phi}}_l\right)^T \mathbf{D}\left(\mathbf{J}_{\theta_l}\tilde{\boldsymbol{\phi}}_l\right). \tag{9}$$

Without loss of generality, the energy in the compensated spectral profile can be normalized to unity

$$\boldsymbol{\phi}_l^T \mathbf{D}\boldsymbol{\phi}_l = 1. \tag{10}$$

It is assumed that the diagonal of $\mathbf{D}$ is a smooth function (which is the typical case in practice, see below) such that the weights applied to the shifted spectral profile, for small shifts, give approximately the same result as do shifting of the weighted spectral profile, i.e.,

$$\mathbf{D}^{\frac{1}{2}}\mathbf{J}_{\theta_l}\tilde{\boldsymbol{\phi}}_l \approx \mathbf{J}_{\theta_l}\widetilde{\left(\mathbf{D}^{\frac{1}{2}}\boldsymbol{\phi}_l\right)}. \tag{11}$$

Then, the shifted and compensated spectral profile has approximately unit energy

$$\left(\mathbf{J}_{\theta_l}\tilde{\boldsymbol{\phi}}_l\right)^T \mathbf{D}\left(\mathbf{J}_{\theta_l}\tilde{\boldsymbol{\phi}}_l\right) \approx 1. \tag{12}$$

The cost function in (9) can be approximated by

$$\mathcal{J}(\theta_l, a_l) \approx \mathbf{q}_l^T \mathbf{D}\mathbf{q}_l - 2a_l \mathbf{q}_l^T \mathbf{D}^{\frac{1}{2}}\mathbf{J}_{\theta_l}\widetilde{\left(\mathbf{D}^{\frac{1}{2}}\boldsymbol{\phi}_l\right)} + a_l^2 \tag{13}$$

which by introducing the weighted spectral profile $\boldsymbol{\xi}_l$

$$\boldsymbol{\xi}_l = \mathbf{D}^{\frac{1}{2}}\boldsymbol{\phi}_l \tag{14}$$

can be rewritten as

$$\mathcal{J}(\theta_l, a_l) \approx \mathbf{q}_l^T \mathbf{D}\mathbf{q}_l - 2a_l \mathbf{q}_l^T \mathbf{D}^{\frac{1}{2}}\mathbf{J}_{\theta_l}\tilde{\boldsymbol{\xi}}_l + a_l^2. \tag{15}$$

The joint minimization with respect to θ_l and a_l can now be performed by first maximizing the second term of (13) using a grid search of θ_l in the interval $[-\Theta, \Theta]$ in order to find the optimum frequency shift

$$\hat{\theta}_l = \arg\max_{\theta_l}\left[\mathbf{q}_l^T \mathbf{D}^{\frac{1}{2}}\mathbf{J}_{\theta_l}\tilde{\boldsymbol{\xi}}_l\right]. \tag{16}$$

Once the frequency shift has been estimated, $\hat{a}_l$ is calculated by minimizing the cost function with respect to a_l

$$\frac{\partial \mathcal{J}(\hat{\theta}_l, a_l)}{\partial a_l} = 0 \tag{17}$$

and the resulting estimate $\hat{a}_l$ is given by

$$\hat{a}_l = \mathbf{q}_l^T \mathbf{D}^{\frac{1}{2}}\mathbf{J}_{\hat{\theta}_l}\tilde{\boldsymbol{\xi}}_l. \tag{18}$$

A measure of how well $\mathbf{q}_l$ fits the model in (6) is determined by the weighted squared error between $\mathbf{q}_l$ and the frequency-shifted, amplitude-scaled spectral profile

$$e_l = \mathcal{J}(\hat{\theta}_l, \hat{a}_l) = \left(\mathbf{q}_l - \hat{a}_l \mathbf{J}_{\hat{\theta}_l}\tilde{\boldsymbol{\phi}}_l\right)^T \mathbf{D}\left(\mathbf{q}_l - \hat{a}_l \mathbf{J}_{\hat{\theta}_l}\tilde{\boldsymbol{\phi}}_l\right). \tag{19}$$

Since this definition is strongly dependent on the amplitude estimate, a normalized model error has been found to be more appropriate

$$e_l' = \frac{e_l}{\hat{a}_l^2}. \tag{20}$$

Design of the Weight Matrix $\mathbf{D}$*:* The logarithmic frequency scale causes the inner product of two spectra to overemphasize the low frequency content. This undesirable property can, however, be corrected for by proper design of the weight matrix $\mathbf{D}$ in (8). In order to determine the weight matrix, the expression for the total energy of a continuous-frequency spectrum $q(f)$ over the frequency interval $[0, f_s]$ is first considered

$$E = \int_0^{f_s} q^2(f) df. \tag{21}$$

Using a Riemann sum approximation, the energy can be approximated by

$$E \approx E_U = \sum_{t=0}^{N-1} q^2(\nu_t)\Delta\nu_t \tag{22}$$

where ν_t denotes the frequency that results from uniform, critical sampling of the spectrum $q(f)$. Since $\Delta\nu_t = f_s/N$, the energy is obtained by

$$E_U = \frac{f_s}{N}\sum_{t=0}^{N-1} q^2(\nu_t). \tag{23}$$

By instead using a Riemann sum approximation for the logarithmically sampled frequency scale f_k in (5), combined with the assumption that the energy below f_0 is zero and $10f_0 = f_s/2$, the energy is obtained by

$$E_L = 2\sum_{k=0}^{K-1} q^2(f_k) f_0 \left(10^{\frac{k}{K}} - 10^{\frac{k-1}{K}}\right). \tag{24}$$

Since we would like E_U and E_L to be identical, the following identity must hold:

$$\frac{f_s}{N}\sum_{t=0}^{N-1} q^2(\nu_t) = 2\sum_{k=0}^{K-1} q^2(f_k) f_0 \left(10^{\frac{k}{K}} - 10^{\frac{k-1}{K}}\right) \tag{25}$$

which also may be written as

$$\sum_{t=0}^{N-1} q^2(\nu_t) = \sum_{k=0}^{K-1} q^2(f_k) d_k \tag{26}$$

where

$$d_k = \frac{N f_0}{f_s}\left(10^{\frac{k}{K}} - 10^{\frac{k-1}{K}}\right). \tag{27}$$

In matrix form, we have that

$$\mathbf{q}_U^H \mathbf{q}_U \approx 2\mathbf{q}^H \mathbf{D}\mathbf{q} \tag{28}$$

where $\mathbf{q}_U$ and $\mathbf{q}$ represent the uniformly and logarithmically sampled spectra, respectively; the weighting factors d_k define the diagonal entries of the desired $\mathbf{D}$. Some additional considerations on how to design $\mathbf{D}$ are presented in Appendix A.

Amplitude Estimate: The average power of a windowed signal segment $\mathbf{x}$ is given by

$$\mathcal{P} = \frac{1}{N}\mathbf{x}^H \mathbf{W}^2 \mathbf{x} \tag{29}$$

which, by Parseval's theorem, can be equally obtained from frequency domain information,

$$\mathcal{P}_U = \frac{1}{N^2}\mathbf{q}_U^H \mathbf{q}_U. \tag{30}$$

In the same way, the signal power can be expressed in terms of the logarithmically sampled spectrum $\mathbf{q}$ such that

$$\mathcal{P}_L = \frac{2}{N^2}\mathbf{q}^H\mathbf{D}\mathbf{q}. \tag{31}$$

Since the scaling factor $2/N^2$ is not included in the WLS criterion in (8), amplitude calculations need to be modified by this factor to become meaningful. Hence, the effective amplitude $\hat{a}_{e,l}$ is calculated from $\hat{a}_l$ by employing the following expression:

$$\hat{a}_{e,l} = \sqrt{\frac{2}{N^2}} \cdot \hat{a}_l. \tag{32}$$

D. Tracking of the Spectral Profile

So far, the spectral profile has been considered as being a priori known in the parameter estimation. It is, however, desirable to have a self-tuning method which adapts the spectral profile to the waveform characteristics of each new patient while also tracking intrapatient waveform changes. The present method is, therefore, implemented in an adaptive fashion where the spectral profile is slowly updated for every new spectrum $\mathbf{q}_l$. The initial spectral profile contains, as earlier stated, a single peak against which $\mathbf{q}_0$ is shifted

$$\boldsymbol{\phi}_0(i) = \begin{cases} 1, & i = p_0 \\ 0.01, & \text{otherwise} \end{cases} \tag{33}$$

where p_0 denotes the position of the fundamental frequency. After θ_l and a_l have been estimated and $\mathbf{q}_l$ shifted to the position of the fundamental frequency in the spectral profile, the spectral profile is updated through exponential averaging, i.e.,

$$\hat{\boldsymbol{\phi}}_{l+1} = (1-\alpha_l)\hat{\boldsymbol{\phi}}_l + \alpha_l \frac{\mathbf{J}_{-\hat{\theta}_l}\tilde{\mathbf{q}}_l}{\left\|\mathbf{J}_{-\hat{\theta}_l}\tilde{\mathbf{q}}_l\right\|}, \quad l > 0 \tag{34}$$

The related energy-compensated and normalized spectral profile is obtained by

$$\hat{\boldsymbol{\xi}}_{l+1} = \frac{\mathbf{D}^{\frac{1}{2}}\hat{\boldsymbol{\phi}}_{l+1}}{\left\|\mathbf{D}^{\frac{1}{2}}\hat{\boldsymbol{\phi}}_{l+1}\right\|}. \tag{35}$$

The gain α_l in (34) is defined by

$$\alpha_l = \beta \cdot z_l \tag{36}$$

where z_l is a *binary signal reliability* variable which is introduced to defer updates in (34) when unreliable signal segments occur; the parameter β defines the adaptation speed. The reliability of a segment is determined by the preprocessing stage which outputs information on beat morphology. A segment is judged to be unreliable when an ectopic beat occurs, and especially for an ectopic beat with a rarely occurring morphology. The variable z_l is set to zero whenever a segment contains a beat for which no valid beat average exists (at least six beats are required for creating a beat average).

The position of the fundamental frequency may be fixed in the spectral profile throughout the analysis of a signal. However, since the fundamental frequency does not change dramatically from segment to segment, the maximum number of shifts Θ needed to evaluate (16) can be substantially reduced by the inclusion of a technique for updating p_0 such that it becomes a function of the segment number l.[1] The technique is based on an exponentially averaged spectrum $\mathbf{s}_l$ computed by

$$\mathbf{s}_l = (1-\rho)\mathbf{s}_{l-1} + \rho\mathbf{q}_l, \quad l > 0 \tag{37}$$

where $\mathbf{s}_0 = \mathbf{q}_0$ and ρ a fixed adaptation gain. Based on $\mathbf{s}_l$, an estimate of the fundamental position for the subsequent segment p_{l+1} is obtained by finding the position of the maximum peak of $\mathbf{s}_l$

$$\hat{p}_{l+1} = \arg\max_i s_l(i). \tag{38}$$

If $\hat{p}_{l+1}$ differs from $\hat{p}_l$, the spectral profile $\hat{\boldsymbol{\phi}}_{l+1}$ needs to be adjusted since its fundamental peak should be positioned at p_{l+1}

$$\hat{\boldsymbol{\phi}}_{l+1} = \begin{cases} \mathbf{J}_{\epsilon_l}\hat{\boldsymbol{\phi}}_l, & \hat{p}_{l+1} \neq \hat{p}_l \\ \hat{\boldsymbol{\phi}}_l, & \hat{p}_{l+1} = \hat{p}_l \end{cases} \tag{39}$$

where

$$\epsilon_l = \hat{p}_{l+1} - \hat{p}_l. \tag{40}$$

Note that the spectral profile, $\boldsymbol{\phi}$, is an exponential average of all spectra after they have been shifted to the position of the fundamental frequency in the spectral profile, while $\mathbf{s}_l$ is a conventional exponentially averaged spectrum.

IV. Spectral Profile Parameters

The definition of a waveform parameter should be such that the shape is decoupled from the fibrillation frequency. One model which exhibits this property is the spectral line model which is a parametric representation of the normalized spectral profile $\boldsymbol{\phi}_l$, defined by the peak amplitude b_l of the fundamental frequency and the exponential decay γ_l (shape parameter) of the M harmonics

$$\phi_l(p_l + h_m) = \begin{cases} b_l e^{-\gamma_l m}, & m = 0, 1, \ldots, M \\ 0, & \text{otherwise.} \end{cases} \tag{41}$$

The parameter M is selected such that only harmonics below 20 Hz are included in the analysis. The parameter h_m denotes the offset position of the m^{th} harmonic in relation to the fundamental frequency at p_l, and is given by

$$h_m = K\left\lfloor \log_{10}(m+1) \right\rfloor \tag{42}$$

where $\lfloor\cdot\rfloor$ denotes rounding to the nearest integer.

The spectral line model can be made linear in its parameters by taking the logarithm of (41) and then employing the least squares cost function

$$J(\ln b_l, \lambda_l) = \sum_{m=0}^{M} \left(\ln\phi_l(p_l + h_m) - (\ln b_l - \gamma_l m)\right)^2. \tag{43}$$

Minimization of this cost function is performed by setting its derivatives with respect to $\ln b_l$ and γ_l equal to zero. The resulting estimators are given by

$$\hat{b}_l = \exp\left(\frac{2(2M'-1)}{M'(M'+1)}\sum_{m=0}^{M}\ln\phi_l(p_l + h_m)\right.$$

[1]The most favorable situation is when the shift interval is centered around the prevailing atrial repetition rate. Depending on where the prevailing rate is located compared to the initial fundamental position, the fundamental position may have to be adjusted for efficient use of the shift interval. The shift interval can then be decreased after adjustment of the fundamental position to the atrial rate.

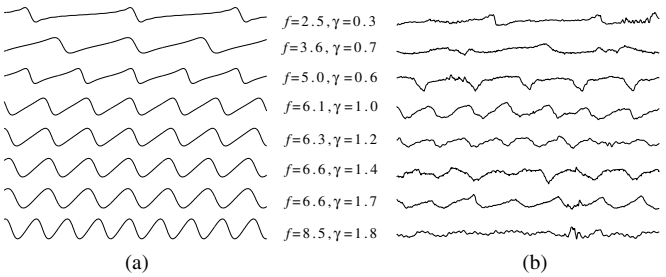

Fig. 2. (a) Simulated signals obtained by the spectral line model in (41). (b) Residual ECG signals containing atrial fibrillation with frequencies and exponential decays matching those in (a). The fundamental frequency f was obtained from the frequency shift parameter. For readability reasons, the signal amplitudes or phases in (a) are not matched to those in (b).

$$-\frac{6}{M'(M'+1)}\sum_{m=0}^{M} m\ln\phi_l(p_l+h_m)\Bigg) \tag{44}$$

and

$$\hat{\gamma}_l = -\frac{6}{M'(M'+1)}\sum_{m=0}^{M}\ln\phi_l(p_l+h_m) + \frac{12}{M'\left((M')^2-1\right)}\sum_{m=0}^{M} m\ln\phi_l(p_l+h_m) \tag{45}$$

where $M' = M+1$.

With the spectral line model introduced in (41), a wide range of shapes can be represented spanning from biphasic P waves, across the characteristic "sawtooth-like shape" of organized atrial flutter/fibrillation and tachycardia, to less organized and more sinusoidal looking atrial fibrillation, see Fig. 2(a). The different model signals were selected such that higher fundamental frequencies are combined with a more sinusoidal shape (i.e., a larger exponential decay) while signals with lower fundamental frequencies were combined with waveforms with sharper edges (i.e., a smaller exponential decay). It may be hypothesized that irregular activation patterns in the atria are subjected to a larger degree of spatial averaging, causing the signal waveforms on the body surface to have a higher fundamental frequency and a smoother shape. On the other hand, regular activation patterns correspond to fewer propagation paths and, therefore, a lower degree of spatial averaging which results in waveforms with sharper edges. The model signals in Fig. 2(a) are contrasted by a variety of atrial signals in Fig. 2(b) taken from the databases described below. For each atrial signal, the exponential decay γ_l is presented, covering a wide range of values.

In addition to the spectral line parameters, the SNR κ_l represents an important feature of each spectral profile, which here is defined as the ratio between the average amplitude of the fundamental frequency and the first harmonic and the noise level in between these two peaks, i.e.,

$$\kappa_l = \frac{\frac{1}{2}\left(\phi_l(p_l)+\phi_l\left(p_l+|\log_{10}2|\right)\right)}{\phi_l\left(p_l+|\log_{10}1.5|\right)}. \tag{46}$$

This parameter is suitable for characterizing different types of atrial activity: the spectral profile exhibits a harmonic pattern when an atrial signal is present whereas the harmonics disappear when a transition occurs to a nonrepetitive signal, and vice versa; in both cases, the fundamental frequency is assumed to be 2.5 Hz or higher. In a recent study, a parameter similar to κ_l was suggested for the purpose of quantifying atrial fibrillation organization, expressed in terms of the ratio of the area under the harmonics to the total area [33].

At this point, we have two different amplitude definitions for characterizing the spectral profile, namely, the normalized peak amplitude b_l of the fundamental frequency as defined by the spectral line model, and the amplitude $a_{e,l}$ which describes the optimal scaling of the spectral profile $\boldsymbol{\phi}_l$ to $\mathbf{q}_l$ in the WLS sense. Although both definitions have their advantages for analysis of harmonic spectra, we have restricted ourselves to only consider $a_{e,l}$ since it offers an over-all characterization of the spectral profile (see Section VII). Since $a_{e,l}$ is the effective amplitude of the signal, and accordingly represents a less useful parameter from a clinical viewpoint, an expression has been derived which relates $a_{e,l}$ to the more intuitive peak amplitude A_l (Appendix B),

$$A_l = a_{e,l}\cdot\sqrt{\frac{2}{1-e^{-2\gamma_l}}} \tag{47}$$

assuming that the spectral line model characterizes the observed signal.

V. Database

In order to investigate the properties of different atrial arrhythmias, the present method was developed using a learning database with ECG signals recorded during different atrial conditions, and evaluated on another database obtained from patients with atrial fibrillation. The learning database contains signals from 40 subjects of which 24 had various types of atrial arrhythmias (two were diagnosed as atrial tachycardia, one as third-degree atrioventricular block (AV block III), one as atrial flutter, and 20 as atrial fibrillation) whereas the remaining 16 were recorded during normal sinus rhythm. The evaluation database contains signals from 211 patients, all clinically diagnosed with atrial fibrillation.

All signals were recorded with the standard 12-lead ECG configuration and had a duration of 1 min. Only lead V_1 was subjected to time-frequency analysis, although V_2 and V_3 were used for QRST cancellation. The signals were digitized at a sampling rate of 1 kHz and an amplitude resolution of 0.6 μV using equipment by Siemens-Elema AB, Sweden.

VI. Results

This section begins by presenting several examples which illustrate the performance of the method on various types of atrial arrhythmias, all taken from the learning database. The properties of different parameter combinations are then investigated on the evaluation database. Table I presents the parameter values used for analyzing the residual ECGs. It should be noted that the maximum frequency shift was initially set to $\Theta = 42$, and later decreased to $\Theta = 25$ after finding the correct average fundamental position so that the shift interval became centered around the fundamental frequency. The parameters A_l, γ_l, and κ_l are presented below as averages of the estimates obtained from the last 20 signal windows, and are denoted with $\overline{A}$, $\overline{\gamma}$, and $\overline{\kappa}$, respectively. In the same way, the fundamental frequency $\overline{f}$ is

TABLE I
PARAMETER VALUES FOR ANALYSIS OF RESIDUAL ECG SIGNALS USING A SAMPLING RATE OF 50 Hz

N	K	L	**W**	f_0 (Hz)	p_0	Θ	β	ρ
128	128	50	Hann.	2.5	42	25	0.05	0.025

obtained from averaging of $f_{\hat{p}_l+\hat{\theta}_l}$. For comparative purposes, the conventional power spectrum, here presented as a magnitude spectrum, of each 1-min signal was obtained with Welch's method [20].

A. Signal Analysis: Examples

The diversity of shapes in atrial signals is illustrated by Fig. 3 where the residual ECG signal is presented for seven different subjects of the learning database; the shapes span the entire range from highly irregular, rapid atrial fibrillation to recurrent P waves during AV block III. Enclosed by these two extremes are rhythms such as atrial tachycardia, slow atrial flutter/fibrillation and atrial fibrillation with sawtooth-like shapes. Figs. 4–7 present the logarithmic STFTs (left panel) that correspond to the signals in Fig. 3. The spectral profile, obtained at the end of the 1-min analysis interval, is presented together with the fitted spectral line model and related values on $\overline{\gamma}$ and $\overline{\kappa}$ (middle panel). The fundamental frequency trend is presented in the right panel.

A typical, rather organized case of atrial fibrillation is shown in Fig. 4(a) with a fundamental frequency of about 6 Hz and a variation within 5–7 Hz. The sawtooth-like shape of the signal in Fig. 3(a) is reflected by the presence of two harmonics in the spectral profile; the exponential decay estimate is found to be $\overline{\gamma} = 1.0$, thus indicating that the shape, as expressed by the spectral line model, is sawtooth-like, cf. Fig. 2. Comparing the spectral profile to the magnitude spectrum, it is evident that the fundamental peak of the former spectrum is narrower and that its harmonics are much more easily discerned. Such a behavior is, of course, expected since the spectral profile represents an average of spectra from successive signal intervals where each individual spectrum, prior to averaging, have been shifted such that the fundamental is optimally aligned to the fundamental frequency of the spectral profile. The SNR estimate $\overline{\kappa} = 6.0$ confirms the presence of an atrial rhythm and indicates that $\overline{\gamma}$ is reliable.

Two additional examples of atrial fibrillation are included with different degrees of organization. The example in Fig. 4(b), corresponding to Fig. 3(b), has a fundamental frequency of about 7 Hz, exhibiting a relatively large variation, and one harmonic which yields the values $\overline{\gamma} = 1.2$ and $\overline{\kappa} = 6.5$. Fig. 4(c) presents an example which is considerably less organized than the previous two examples. The fundamental frequency is higher (8.5 Hz) and the absence of harmonics, as indicated by $\overline{\gamma} = 1.8$, implies that the signal is more sinusoidal-looking; the low SNR is reflected by $\overline{\kappa} = 3.1$, cf. Fig. 3(c). In the last two examples in Fig. 4(b) and (c), a large variation of the fundamental frequency causes a marked difference between the spectral profile and the power spectrum.

Fig. 5 presents an unusual case of irregular atrial fibrillation suddenly interrupted by a short segment of highly regular activity. This segment is distinguished by the constant fundamental frequency of about 5 Hz, whereas the variation is within

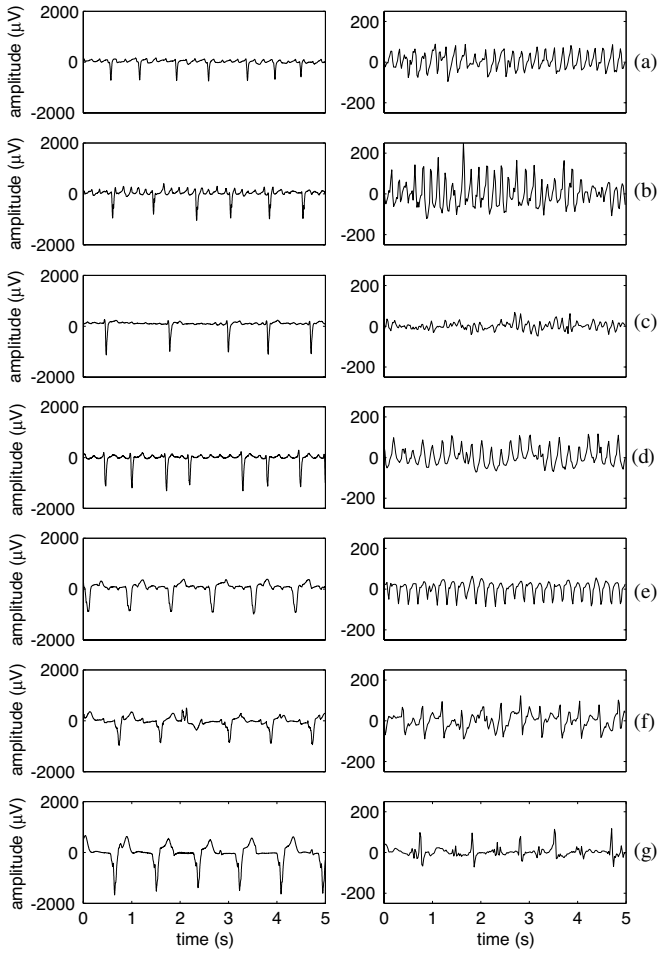

Fig. 3. Five-second excerpts from seven different residual ECG signals with (a), (b), and (d) slow and sawtooth-shaped atrial fibrillation, (c) highly irregular and rapid atrial fibrillation, (e) atrial flutter, (f) pulse-shaped atrial tachycardia, and (g) AV block III.

4–6 Hz for the irregular part of the signal. Similar to the case in Fig. 4(a), two harmonics are observed in the spectral profile resulting in the same exponential decay, i.e., $\overline{\gamma} = 1.0$. When comparing the signals of Fig. 3(a) and (d), it is evident that the f wave shape, without regard to repetition rate, is approximately the same for these two cases.

Fig. 6 presents two examples, one of atrial flutter and one of atrial tachycardia, which differ considerably from the previous examples of fibrillation by having a more stable fundamental frequency and a larger number of harmonics. For the example in Fig. 6(a), the exponential decay is $\overline{\gamma} = 0.6$ which, thus, reflects a rather pulse-shaped biphasic signal, cf. Fig. 3(e); the SNR is high with a value of $\overline{\kappa} = 15.3$. Since this rhythm is regular, the power spectrum and the spectral profile are almost identical. The other example (atrial tachycardia) in Fig. 6(b) exhibits a very low fundamental frequency of about 2.5 Hz, i.e., the lowest possible frequency which can be analyzed by the present parameter settings. The exponential decay is as low as $\overline{\gamma} = 0.3$ and is due to the even more transient type of waveform shape, cf. Fig. 3(f). It should be noted that γ_l is normalized to both fundamental frequency and amplitude, implying that a signal with higher fundamental frequency and higher exponential decay actually can appear to have steeper edges than a signal with lower

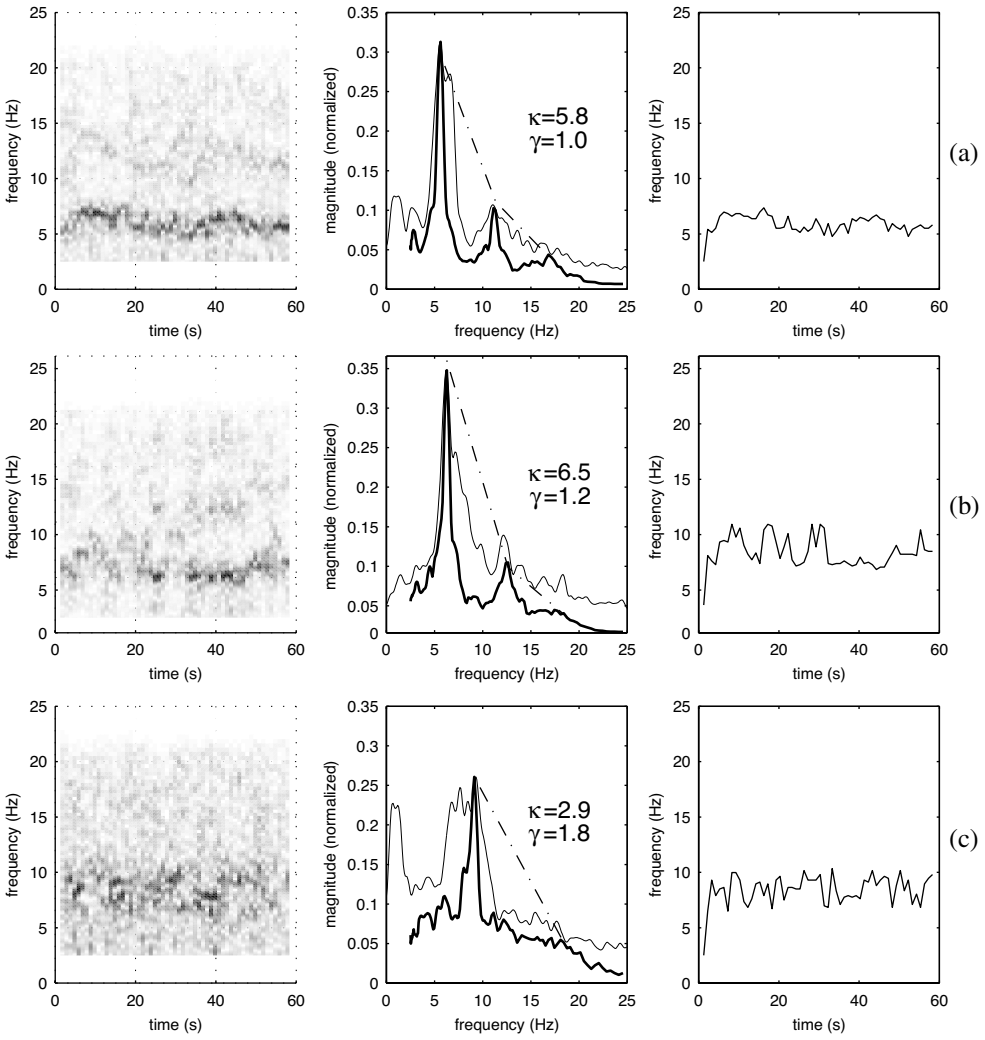

Fig. 4. Analysis of 1-min signals with atrial fibrillation producing a logarithmic STFT (left panel), the spectral profile, the fitted spectral line model and the conventional magnitude spectrum plotted with thick solid, dashed and thin solid lines, respectively (middle panel), and the fibrillation frequency trend (right panel). (a) The spectral profile has a relatively large first harmonic, and a variation in fundamental frequency within 5–7 Hz. (b) As in (a) but with a larger frequency variation. (c) A high fundamental frequency coupled to a large variation (7–10 Hz).

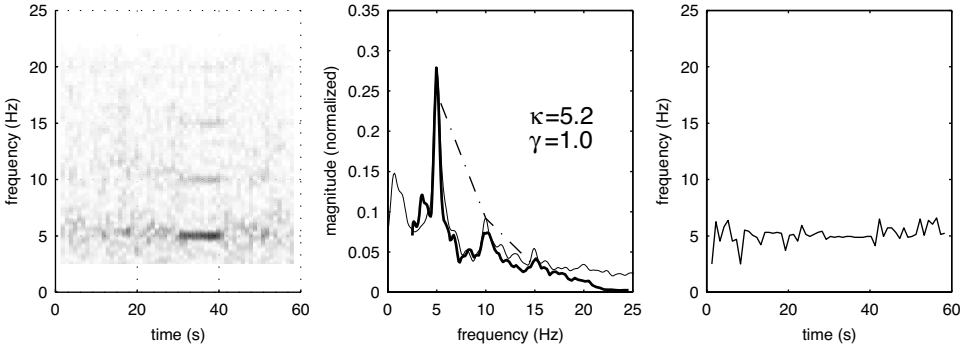

Fig. 5. Analysis of a 1-min signal with atrial fibrillation containing an interval with a highly regular rhythm during second 30 to 40.

frequency and lower exponential decay. Similarly, if the amplitude is higher, the edges appear sharper.

Fig. 7 presents the results from analysis of an ECG with AV block III. Similar to when performing QRST cancellation on a sinus rhythm signal, the P waves are present in the residual ECG. The P wave repetition rate is below the lower limit of 2.5 Hz, see Fig. 3(g). With no fundamental frequency in the allowed range, the frequency shift estimation ceases to function properly and, as a result, no meaningful information is conveyed by the spectral profile—a property described by an SNR of only $\overline{\kappa} = 1.9$ being far too low for representing a harmonic signal.

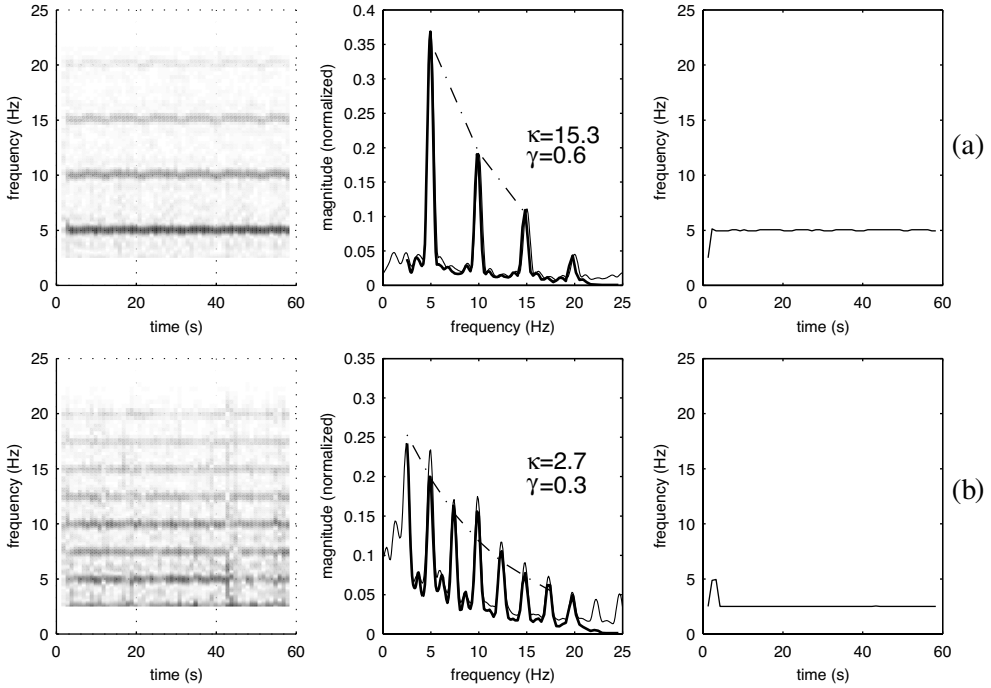

Fig. 6. Analysis of 1-min signals with (a) atrial flutter and (b) atrial tachycardia having very stable fundamental frequencies and several harmonics. The fundamental frequencies are about 5 Hz, and 2.5 Hz, respectively.

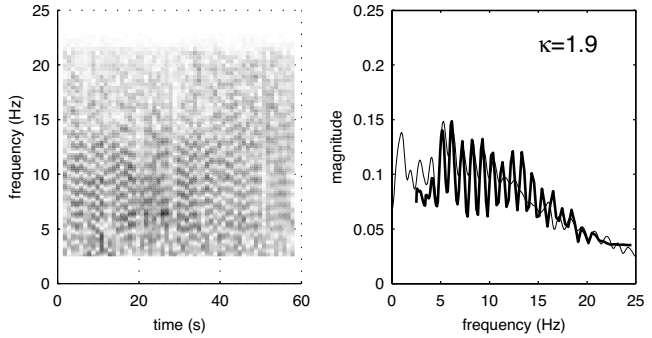

Fig. 7. Analysis of a 1-min signal with AV block III whose fundamental frequency is below the lower limit of 2.5 Hz. As a result, the method cannot produce a meaningful estimate of the spectral profile. The logarithmic STFT displays harmonics due to the P waves contained in the time window.

B. Performance Issues

For each segment, the sequential analysis of the residual ECG produces a set of parameter estimates. However, the resulting parameter trends will track changes in signal characteristics quite differently depending on the time constant associated with the cost function that is used:

- estimates of the amplitude a_l and frequency shift θ_l, resulting from the cost function in (8), are capable of tracking faster segment-to-segment changes;
- estimates of the spectral line model parameters b_l and γ_l, resulting from (43), and the related SNR κ_l, track slower variations in signal characteristics due to the slower update of the spectral profile.

The tracking performance is illustrated by Fig. 8 where a number of parameter trends for the example in Fig. 5 are presented; this particular example is well-suited for illustrating tracking behavior since the signal contains an intermittent change in rhythm characteristics. The most important observation to be made is that all trends (and, consequently, the spectral profile) have converged after about 20 to 30 s, as controlled by the adaptation gain β in the spectral profile update in (34) and (36). This, rather long, time span represents the delay in adjusting to a new shape, and is usually acceptable since variations in shape are often much slower than those in amplitude and frequency.

Fig. 8(a) demonstrates that the estimate of the effective amplitude $\hat{a}_{e,l}$ reacts instantaneously to changes in signal amplitude which occur when the regular rhythm is initiated at second 30, ending 10 s later. In the same way, the frequency estimate responds instantaneously to frequency variations in the input signal. Since the frequency estimator works relative to the available spectral profile, including the position of the fundamental frequency, it produces reliable estimates already at startup although the algorithm has not yet converged to the actual spectral profile, see Fig. 8(b). As can be seen from Fig. 8(c), the normalized model error e'_l, which describes how well each spectrum $\mathbf{q}_l$ fits the amplitude-scaled and frequency-shifted spectral profile, is not influenced by the amplitude change.

The parameters γ_l, b_l, and κ_l are obtained from the spectral profile and are, therefore, dependent on the adaptation gain β; in this study, β was selected to yield a delay of about 10 s. The slower tracking is illustrated by the trends in Fig. 8(d)–(f). For example, the sudden increase in SNR at second 30 (cf. the STFT of the left panel of Fig. 5) is not reflected in the κ_l trend until the interval with a regular rhythm is about to end.

Another performance issue is the degree of improvement achieved by the amplitude estimator when a properly designed weight matrix $\mathbf{D}$ is used in the WLS criterion. Without compensation for spectral oversampling, the method overestimates

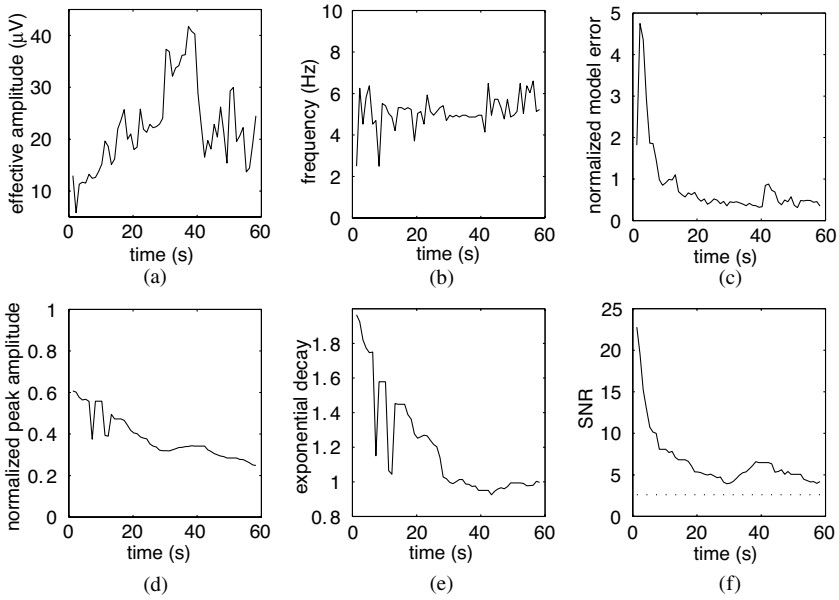

Fig. 8. Parameter trends for the estimates of (a) the effective amplitude $A_{e,l}$, (b) the fundamental frequency $f_{p_l+\theta_l}$, (c) the normalized model error e'_l, (d) the amplitude b_l, (e) the exponential decay γ_l, and (f) the SNR κ_l. The trends are based on the case presented in Fig. 5.

the amplitude, whereas the effective amplitude is correctly estimated when compensation with $\mathbf{D}$ is included. The amplitude estimate is found to be more accurate when the model error is small, see the amplitude trends in Fig. 9(a) obtained from a case with atrial flutter. For less regular rhythms, the model does not equally well account for each signal segment and, therefore, the amplitude estimates become underestimated as illustrated by Fig. 9(b). An underestimated amplitude is also obtained during the startup phase of the algorithm when the spectral profile has not yet adapted to the signal spectrum.

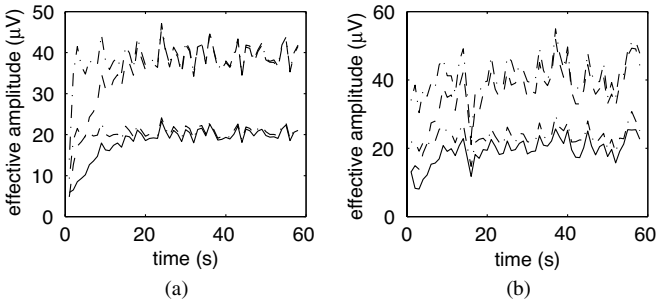

Fig. 9. Effective amplitude estimates produced by the method compared to the true values (obtained from the time domain signal segments) obtained with and without energy compensation (solid line—effective amplitude estimate with energy compensation, dashed—effective amplitude estimate without energy compensation, and dotted lines—true effective amplitude with and without energy compensation). The two signal examples have been presented in (a), Fig. 3(e) and (b) Fig. 3(a).

C. Signal-to-Noise Ratio Threshold

Since signals with an SNR that fall below a certain threshold value must be excluded from further analysis, the learning database was analyzed in order to select a suitable value. Fig. 10 presents the fundamental frequency versus the SNR for the 40 subjects of the learning database, using markers for the different rhythm types. By selecting the threshold to 2.7, all subjects diagnosed with atrial fibrillation/flutter or tachycardia were included except for three subjects where either no atrial signal was discernible (two subjects) or the QRST cancellation failed due to a too high ventricular rate (one subject). With this particular threshold value, three of the subjects with P wave rhythms exceeded the threshold value, see Fig. 10.

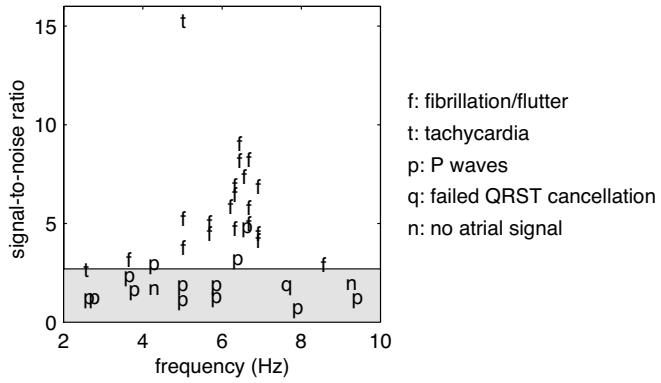

Fig. 10. Fibrillation frequency versus SNR for subjects in the learning database. The area below the selected threshold of 2.7 is shaded.

D. Parameter Properties

We will now investigate potential interrelationships between the fundamental frequency $\overline{f}$ and three different parameters produced by the present method: the amplitude $\overline{A}$, the standard deviation of the fundamental frequency $\sigma_{\overline{f}}$, and the exponential decay $\overline{\gamma}$ describing shape. Before presenting the scattergrams that results from analysis of the evaluation database, we exclude cases with a $\overline{\kappa}$ lower than 2.7, see Fig. 11(a); 30 out of the 211 cases of atrial fibrillation were found to have such a low SNR. The exclusion step accounts for cases that do not contain a repetitive signal for which the spectral profile exhibits a sufficiently distinct fundamental frequency. The diagnosis "atrial fibrillation" may, however, still be valid since it can be based on other

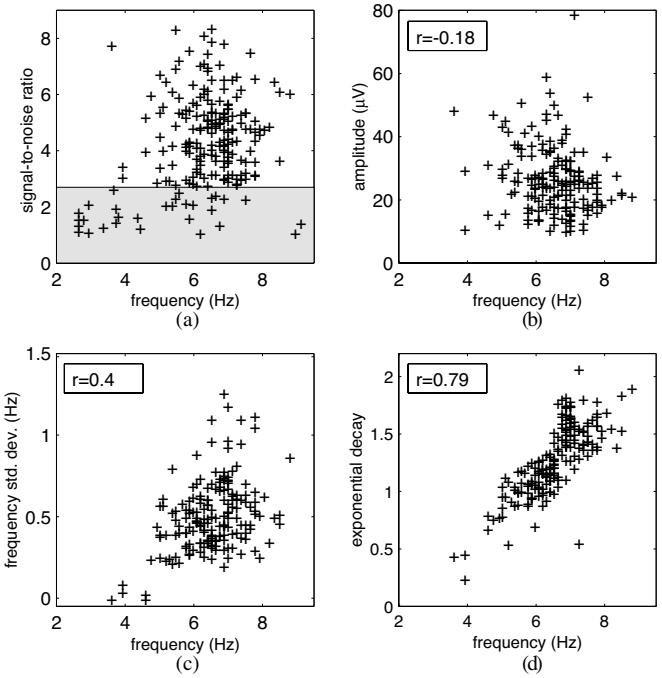

Fig. 11. (a) SNRs $\overline{\kappa}$ below 2.7 are judged too weak to be analyzed. The fundamental frequency is shown versus (b) amplitude $\overline{A}$, (c) variance in fundamental frequency $\sigma_{\overline{f}}$, and (d) exponential decay $\overline{\gamma}$; in each diagram, the correlation coefficient r is presented.

ECG characteristics including an irregular RR interval pattern and the absence of P waves.

For each of the three parameter combinations, the resulting scattergram is presented in Fig. 11(b)–(d) and is based on the remaining 181 cases of atrial fibrillation. No strong interrelationship seems to exist between the fundamental frequency and the parameters $\overline{A}$ and $\sigma_{\overline{f}}$, see Fig. 11(b)–(c), as indicated by the correlation coefficients of -0.18 and 0.4, respectively. From Fig. 11(c) it is obvious that five cases, with fundamental frequencies below 4.5 Hz, have very small standard deviations $\sigma_{\overline{f}}$, i.e., less than 0.1 Hz, possibly suggesting that these cases should rather have been labeled with atrial flutter or tachycardia. For the remaining 176 cases, the fundamental frequency is within the interval 4.5–9 Hz, and with a standard deviation $\sigma_{\overline{f}}$ ranging from 0.2 to 1.5 Hz.

Fig. 11(d) shows that a rather strong correlation exists (correlation coefficient of 0.79) between fundamental frequency and exponential decay: slower fibrillation rhythms are associated with waves having a sharper shape, as described by several harmonics, whereas faster rhythms are associated with waves having a more sinusoidal shape (no harmonics).

VII. Discussion

An important purpose with the present study has been to introduce a new method which robustly estimates fibrillation frequency by making use of the entire spectrum rather than only the amplitude of the fundamental frequency, as was done in our earlier XWVD-based method [31]. By neglecting the harmonics in the estimation process, valuable signal information is lost. Another important purpose has been to remedy the lack of signal processing tools for characterizing the shape of f waves, a tool which may help to better understand the basic mechanisms behind atrial fibrillation. The clinical value of the present shape characterization remains, however, to be established by a series of future studies. Yet another purpose of the present study has been to develop a set of parameters representative for various types of atrial signals being useful for automated arrhythmia classification. The parameter set is here expressed as a number of detailed trends—frequency, amplitude, shape, and SNR—from which additional parameters can be derived.

The main motivation for introducing $\mathbf{D}$ is to weight all frequencies of the spectrum equally in the estimation process. By omitting $\mathbf{D}$ the frequency estimator becomes too focused on lower frequencies and, consequently, more influenced by the fundamental frequency than by the harmonics. Another motivation is to estimate the effective amplitude $a_{e,l}$ accurately, an estimate which then could be related to the peak amplitude A_l through the exponential decay of the spectral line model. The amplitude estimate should ultimately be modified in order to account for the influence of the signal window $\mathbf{W}$ in (2) however, such a modification was not considered necessary since the present study is comparative in nature.

The selection of the spectral profile adaptation gain β is, in general, a trade-off between robustness and tracking capability. A possible modification of the algorithm in order to achieve faster tracking is to use the normalized model error for controlling the adaptation gain. In that way, the tracking could be made faster at startup when the model error is large or when sudden changes occur in shape. The spectral profile is updated only with respect to magnitude, thus ignoring phase information, under the assumption that the different shapes have harmonics with the same phase as the fundamental. As a result, shapes with the same harmonic amplitudes but different harmonic phases cannot be discriminated. An alternative to adaptively updating the spectral profile is to employ principal component decomposition of the entire time-frequency distribution to find a representative spectral profile [34].

It was earlier stated that a large exponential decay corresponds to more sinusoidal shapes. It should be noted, however, that the shape estimation has a slow time constant and, therefore, the shape description should be interpreted in "average" terms. Thus, a sinusoidal shape implies that the signal, in average, has no harmonics, thereby reflecting a less organized signal which does not necessarily exhibit rounder shapes in each and every individual wave.

The normalized peak amplitude b_l quantifies the amplitude of the fundamental frequency of the normalized spectral profile (with unit energy). A value of b_l close to one indicates that the spectral profile contains a single, narrow peak while a lower value corresponds to either a larger number of harmonics or wider peaks. The parameter b_l was not further analyzed in the present study but may, if compensated for by the number of harmonics and the exponential decay, be used as an indicator of width of the spectral peaks. This width may, in turn, be interpreted as a measure of regularity within the signal window for spectral analysis.

The present method is based on the assumption that the exponential decay has a relatively long time constant while rapid

variations in frequency and signal amplitude may occur. Therefore, small variations in shape caused by rapid frequency variation will not significantly affect the estimation procedure. Due to that the spectral profile is an averaged quantity, the method is relatively forgiving to violations of this assumption.

We would like to point out that the presented method relies on successful preprocessing including prefiltering, beat detection, beat classification and extraction of the atrial activity from the surface ECG. For the latter purpose, the improved performance achieved by spatiotemporal QRST cancellation was essential for the outcome of the present study.

The left atrium appears in recent studies to be the most important source of atrial fibrillation [35]–[37], and related to the location of the pulmonary veins [38]. Although the present study is focused on the analysis of lead V_1, mainly reflecting the activity of the right atrium, the novel spectral characterization technique can be equally applied to other leads which better reflect the left atrium.

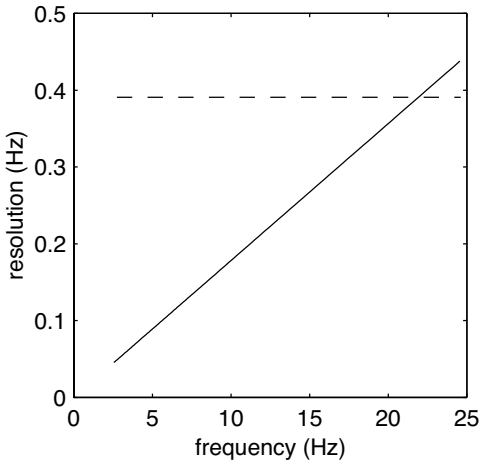

Fig. 12. The increment for uniform frequency sampling is fixed and equals f_s/N (dashed line). The increment for logarithmic frequency (solid line) sampling increases linearly and yields oversampling for most frequencies, except for those above 22 Hz.

APPENDIX A
POWER APPROXIMATION USING THE WEIGHT MATRIX $\mathbf{D}$

For the observations $\mathbf{x}$, the spectrum $\mathbf{q}_U$ is calculated using the $N \times N$ DFT matrix $\mathbf{F}_U$ uniformly sampled within the frequency interval $[0, f_s]$, i.e.,

$$\mathbf{q}_U = \mathbf{F}_U \mathbf{W} \mathbf{x}. \tag{48}$$

Similarly, the logarithmically sampled spectrum $\mathbf{q}$ is calculated by

$$\mathbf{q} = \mathbf{F} \mathbf{W} \mathbf{x}. \tag{49}$$

The average signal power calculated from the spectrum is for these two cases

$$\mathcal{P}_U = \frac{1}{N^2} \mathbf{q}_U^H \mathbf{q}_U = \frac{1}{N^2} \mathbf{x}_l^H \mathbf{W} \mathbf{F}_U^H \mathbf{F}_U \mathbf{W} \mathbf{x}_l, \tag{50}$$

and from (28)

$$\mathcal{P}_L = \frac{2}{N^2} \mathbf{q}^H \mathbf{D} \mathbf{q} = \frac{2}{N^2} \mathbf{x}^H \mathbf{W} \mathbf{F}^H \mathbf{D} \mathbf{F} \mathbf{W} \mathbf{x}. \tag{51}$$

respectively. The two average power values are identical under the assumptions that: 1. the logarithmic frequency scale covers $[f_0, f_{K-1}]$, 2. no energy is contained below f_0, 3. the logarithmic frequency scale oversamples the spectrum, and 4. the weight matrix $\mathbf{D}$ is selected as specified. The distance between successive frequency samples are for the uniform and logarithmic frequency scales shown in Fig. 12. It is noted that the logarithmic spectrum is about eight times oversampled for the lowest frequencies whereas it is slightly undersampled above 22 Hz. The undersampling is, however, uncritical since the signal energy is negligible in this band.

In order to show that (50) and (51) under the above assumptions are equal, it is noted that the DTFT $X(e^{j\omega})$ of an arbitrary signal $x(n)$ with length N can be expressed in terms of the uniformly sampled DFT $X_U(m)$ since

$$\begin{aligned} X(e^{j\omega}) &= \sum_{n=0}^{N-1} x(n) e^{-j\omega n} \\ &= \frac{1}{N} \sum_{n=0}^{N-1} \left[\sum_{m=0}^{N-1} X_U(m) e^{\frac{j2\pi mn}{N}} \right] e^{-j\omega n} \\ &= \sum_{m=0}^{N-1} r(\omega, m) X_U(m), \end{aligned} \tag{52}$$

where

$$r(\omega, m) = \frac{1}{N} \frac{\sin\left(\frac{\omega N - 2\pi m}{2}\right)}{\sin\left(\frac{\omega N - 2\pi m}{2N}\right)} \cdot e^{-j\left[\omega - \left(\frac{2\pi m}{N}\right)\right]\left[\frac{(N-1)}{2}\right]}. \tag{53}$$

Hence, the spectrum for any frequency ω can be computed as a linear combination of the uniformly spaced frequency samples of the N-point DFT.

With the assumption that $\omega_k = 2\pi f_k$ represents a logarithmic scale, the DFT matrix $\mathbf{F}$ can be expressed as the product of a resampling matrix $\mathbf{R}$ and $\mathbf{F}_U$,

$$\mathbf{F} = \mathbf{R} \mathbf{F}_U, \tag{54}$$

where the elements of $\mathbf{R}$ are defined by

$$[\mathbf{R}]_{km} = r(\omega_{k-1}, m-1) \tag{55}$$

for $k = 1, \ldots, K, m = 1, \ldots, N$. It should be noted that $\mathbf{F}$ differs from $\mathbf{F}_U$ in the sense that positive frequencies contained in the interval $[f_0, f_{K-1}]$ are only considered. Therefore, since the frequency content below f_0 is negligible and $f_{K-1} = f_s/2$, a factor of two must be included in order to account for the power of the mirrored, negative frequencies. Using the relationship in (54), the signal power $\mathcal{P}_L$ can be written as

$$\mathcal{P}_L = \frac{2}{N^2} \mathbf{x}^H \mathbf{W} \mathbf{F}_U^H \mathbf{R}^H \mathbf{D} \mathbf{R} \mathbf{F}_U \mathbf{W} \mathbf{x}. \tag{56}$$

It is straightforward to show numerically that $\mathbf{R}^H\mathbf{R}$ has a strong diagonally dominant structure; the off-diagonal elements are several order of magnitudes smaller than those in the diagonal. Since the elements of a column in $\mathbf{R}$ describes how much the uniformly sampled frequencies are needed for representing f_k, the diagonal elements of $\mathbf{R}^H\mathbf{R}$ describe the over- or underrepresentation of the uniformly sampled frequencies. By choosing the diagonal entries d_k of $\mathbf{D}$ as suggested above, the product $\mathbf{R}^H\mathbf{D}\mathbf{R}$ becomes essentially equal to the identity matrix for frequencies in the interval $[f_0, f_{K-1}]$, and, as a result, will eliminate the undesirable effects due to logarithmic sampling. The two matrices $\mathbf{R}^H\mathbf{R}$ and $\mathbf{R}^H\mathbf{D}\mathbf{R}$ are presented in Fig. 13(a) and (b), respectively, from where it can be observed that the compensated matrix $\mathbf{R}^H\mathbf{D}\mathbf{R}$ is essentially an identity matrix within $[f_0, f_{K-1}]$. Fig. 13(c) displays the diagonal elements of $\mathbf{R}^H\mathbf{R}$ and $\mathbf{R}^H\mathbf{D}\mathbf{R}$, respectively; the edge phenomena that occurs in $\mathbf{R}^H\mathbf{D}\mathbf{R}$ above 22 Hz is due to spectral undersampling but has negligible influence in practice.

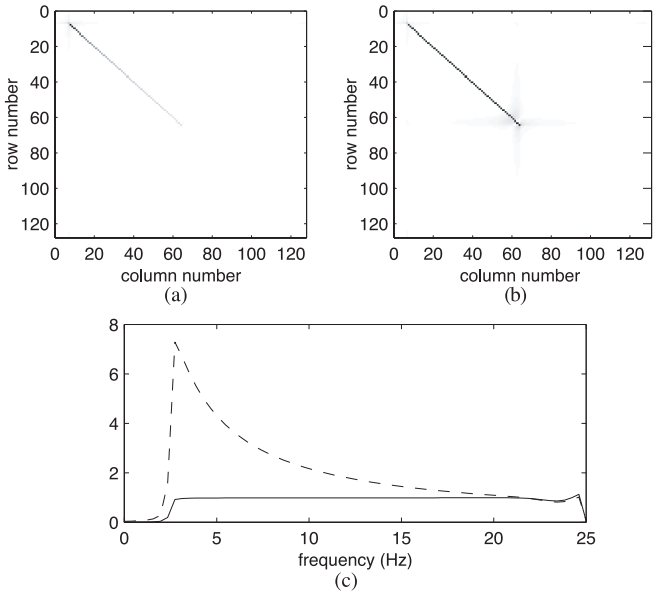

Fig. 13. The matrices (a) $\mathbf{R}^H\mathbf{R}$, and (b) $\mathbf{R}^H\mathbf{D}\mathbf{R}$ plotted as grey-scale images, and (c) the diagonal elements of the matrices in (a) and (b).

Appendix B
Peak Amplitude Estimation

For most clinicians, the peak amplitude defines the amplitude of a waveform rather than the effective amplitude as obtained by the estimator in (18). For example, P waves and atrial fibrillation may have very different effective amplitudes although their peak amplitudes are identical. It is, therefore, highly desirable to derive an expression which relates the effective amplitude to the peak amplitude assuming that the waveform exhibits a certain, model-defined shape. Such an expression can be derived for the spectral line model which in a continuous-time context is given by

$$x(t) = -\sum_{k=1}^{\infty} e^{-\gamma(k-1)} \sin \Omega_0 k t = \frac{-e^{-\gamma} \sin \Omega_0 t}{1 + e^{-2\gamma} - 2e^{-\gamma} \cos \Omega_0 t}, \tag{57}$$

where Ω_0 is the fundamental frequency. As before, the parameter γ defines the exponential decay of the harmonics. The peak amplitude of this model is, for different values of γ, obtained by setting its derivative with respect to t equal to zero. The value of t corresponding to the maximum (or minimum) of each period is then inserted into the model resulting in the peak (absolute) amplitude

$$a_p = \frac{1}{1 - e^{-2\gamma}}. \tag{58}$$

The effective amplitude for the signal in (57) is given by

$$a_e = \sqrt{\int_0^{\frac{2\pi}{\Omega_0}} x^2(t) dt} = \frac{1}{\sqrt{2(1 - e^{-2\gamma})}}. \tag{59}$$

Thus, for a given shape represented by γ and estimated by (45), the ratio between the peak and effective amplitude is given by

$$A_p = a_e \sqrt{\frac{2}{1 - e^{-2\gamma}}}. \tag{60}$$

It should be noted that this expression neglects the influence of windowing, an operation which was part of the short-term Fourier transform in (2). For the discrete-time evaluation, the sample closest to the t of the maximum (or minimum) is selected.

Acknowledgment

The authors would like to thank Prof. P.-O. Börjesson for stimulating discussions.

References

[1] N. M. Wheeldon, "Atrial fibrilation and anticoagulant therapy," *Eur. Heart J.*, vol. 16, pp. 302–312, 1995.
[2] W. Feinberg, J. Blackshear, A. Laupacis, R. Kronmal, and R. Hart, "Prevalence, age distribution, and gender of patients with atrial fibrillation. Analysis and implications," *Arch. Intern. Med.*, vol. 13, pp. 469–473, 1995.
[3] C. Furberg, B. Psaty, T. Manolio, J. Gardin, V. Smith, and P. Rautaharju, "Prevalence of atrial fibrillation in elderly subjects (the cardiovascular health study)," *Amer. J. Cardiol.*, vol. 74, pp. 236–241, 1994.
[4] G. Moe, "On the multiple wavelet hypothesis of atrial fibrillation," *Arch. Int. Pharmacodyn. Ther.*, vol. 140, pp. 183–188, 1962.
[5] M. A. Allessie, W. J. Lammers, F. I. Bonke, and J. M. Hollen, "Experimental evaluation of Moe's multiple wavelet hypothesis of atrial fibrillation," in *Cardiac Electrophysiology and Arrhythmias*, J. Jaliff and D. Zipes, Eds. Orlando, FL: Grune & Stratton, 1985, pp. 265–275.
[6] K. Konings, C. Kirchhof, J. Smeets, H. Wellens, O. Penn, and M. Allessie, "High-density mapping of electrically induced atrial fibrillation in humans," *Circ.*, vol. 89, pp. 1665–1680, 1994.

[7] P. Rensma, M. Allessie, W. Lammers, F. Bonke, and M. Schalij, "Length of excitation wave and susceptibility to reentrant atrial arrhythmias in normal conscious dogs," *Circ. Res.*, vol. 62, no. 2, pp. 395–410, 1988.
[8] A. Capucci, M. Biffi, and G. Boriani, "Dynamic electrophysiological behavior of human atria during paroxysmal atrial fibrillation," *Circ.*, vol. 92, no. 1, pp. 1193–1202, 1995.
[9] K. B. Kim, M. D. Rodefeld, R. B. Schuessler, J. L. Cox, and J. P. Boineau, "Relationship between local atrial fibrillation interval and refractory period in the isolated canine atrium," *Heart*, vol. 94, no. 1, pp. 2961–2967, 1996.
[10] M. Holm, R. Johansson, S. B. Olsson, J. Brandt, and C. Lührs, "A new method for analysis of atrial activation during chronic atrial fibrillation in man," *IEEE Trans. Biomed. Eng.*, vol. 43, pp. 198–210, Feb. 1996.
[11] G. Botteron and J. Smith, "Quantitative assessment of the spatial organization of atrial fibrillation in the human heart," *Circ.*, vol. 93, pp. 513–518, 1996.
[12] A. Goette, C. Honeycutt, and J. Langberg, "Electrical remodeling in atrial fibrillation. Time course and mechanism," *Circ.*, vol. 94, no. 11, pp. 1968–2974, 1996.
[13] M. Wijffels, C. Kirchhof, R. Dorland, and M. Allessie, "Atrial fibrillation begets atrial fibrillation. A study in awake chronically instrumented goats," *Circ.*, vol. 92, no. 7, pp. 1954–1968, 1995.
[14] R. Tieleman, C. D. Langen, I. V. Gelder, P. de Kam, J. Grandjean, K. Bel, M. Wijffels, M. Allessie, and H. Crijns, "Verapamil reduces tachycardia-induced electrical remodeling of the atria," *Circ.*, vol. 95, no. 7, pp. 1945–1953, 1997.
[15] M. Thurmann and J. Janney, "The diagnostic importance of fibrillatory wave size," *Circ.*, vol. 25, pp. 991–994, 1966.
[16] G. Wagner, *Practical Electrocardiography*, 9th ed. Baltimore, MD: Williams & Wilkins, 1994.
[17] D. S. Rosenbaum and R. J. Cohen, "Frequency based measures of atrial fibrillation in man," in *Proc. EMBS*, 1990, pp. 582–583.
[18] J. Slocum, A. Sahakian, and S. Swiryn, "Diagnosis of atrial fibrillation from surface electrocardiograms based on computer-detected atrial activity," *J. Electrocardiol.*, vol. 25, pp. 1–8, 1992.
[19] A. Bollmann, N. Kanuru, K. McTeague, P. Walter, D. DeLurgio, and J. Langberg, "Frequency analysis of human atrial fibrillation using the surface electrocardiogram and its response to ibutilide," *Amer. J. Cardiol.*, vol. 81, pp. 1439–1445, 1998.
[20] M. Holm, S. Pehrsson, M. Ingemansson, L. Sörnmo, R. Johansson, L. Sandhall, M. Sunemark, B. Smideberg, C. Olsson, and S. B. Olsson, "Non-invasive assessment of atrial refractoriness during atrial fibrillation in man—introducing, validating and illustrating a new ECG method," *Cardiovasc. Res.*, vol. 38, pp. 69–81, 1998.
[21] Q. Xi, A. Sahakian, and S. Swiryn, "The influence of QRS cancellation on signal characteristics of atrial fibrillation in the surface electrocardiogram," in *Proc. Comput. Cardiol.*, 2002.
[22] J. Slocum, E. Byrom, L. McCarthy, A. Sahakian, and S. Swiryn, "Computer detection of atrioventricular dissociation from surface electrocardiograms during wide QRS complex tachycardia," *Circ.*, vol. 72, pp. 1028–1036, 1985.
[23] S. Shkurovich, A. Sahakian, and S. Swiryn, "Detection of atrial activity from high-voltage leads of implantable ventricular defibrillators using a cancellation technique," *IEEE Trans. Biomed. Eng.*, vol. 45, pp. 229–234, Feb. 1998.
[24] M. Stridh and L. Sörnmo, "Spatiotemporal QRST cancellation techniques for improved characterization of atrial fibrillation in the surface ECG," in *Proc. 19th Annu. IEEE/EMBS Conf.*, vol. 1, 1997, pp. 48–49.
[25] ——, "Spatiotemporal QRST cancellation techniques for analysis of atrial fibrillation," *IEEE Trans. Biomed. Eng.*, vol. 48, pp. 105–111, Jan. 2001.
[26] P. Langley, J. P. Bourke, and A. Murray, "Frequency analysis of atrial fibrillation," in *Proc. Comput. Cardiol.*, 2000, pp. 65–68.
[27] J. J. Rieta, V. Zarzoso, J. Millet Roig, R. Garcia Civera, and R. Ruiz Granell, "Atrial activity extraction based on blind source separation as an alternative QRST cancellation for atrial fibrillation analysis," in *Proc. Comput. Cardiol.*, 2000, pp. 69–72.
[28] C. Vásquez, A. Hernández, F. Mora, G. Carrault, and G. Passariello, "Atrial activity enhancement by Wiener filtering using an artificial neural network," *IEEE Trans. Biomed. Eng.*, vol. 48, pp. 940–944, Aug. 2001.
[29] J. Waktare, K. Hnatkova, C. Meurling, H. Nagayoshi, T. Janota, A. Camm, and M. Malik, "Optimal lead configuration in the detection and subtraction of QRS and T wave templates in atrial fibrillation," in *Proc. Comput. Cardiol.*, 1998, pp. 629–632.
[30] P. Langley, M. Stridh, J. J. Rieta, L. Sörnmo, J. Millet-Roig, and A. Murray, "Comparison of atrial rhythm extraction techniques for the estimation of the main atrial frequency from the 12-lead electrocardiogram in atrial fibrillation," in *Proc. Comput. Cardiol.*, 2002, pp. 29–32.
[31] M. Stridh, L. Sörnmo, C. J. Meurling, and S. B. Olsson, "Characterization of atrial fibrillation using the surface ECG: time-dependent spectral properties," *IEEE Trans. Biomed. Eng.*, vol. 48, pp. 19–27, Jan. 2001.
[32] T. Everett, L. Kok, R. Vaughn, R. Moorman, and D. Haines, "Frequency domain algorithm for quantifying atrial fbrillation organization to increase defibrillation efficiency," *IEEE Trans. Biomed. Eng.*, vol. 48, pp. 969–978, Sept. 2001.
[33] T. Everett, R. Moorman, L. Kok, J. Akar, and D. Haines, "Assessment of global atrial fibrillation organization to optimize timing of atrial defibrillation," *Circ.*, vol. 103, pp. 2857–2861, 2001.
[34] S. H. Nawab, D. M. Beyerbach, and E. Dorken, "Principal decomposition of time-frequency distributions," *IEEE Trans. Signal Processing*, vol. 41, pp. 3182–3186, Nov. 1993.
[35] R. Mandapati, A. Skanes, J. Chen, O. Berenfeld, and J. Jalife, "Stable microreentrant sources as a mechanism of atrial fibrillation in the isolated sheep heart," *Circ.*, vol. 101, pp. 194–199, 2000.
[36] M. Mansour, R. Mandapati, O. Berenfeld, J. Chen, F. Samie, and J. Jalife, "Left-to-right gradient of atrial frequencies during acute atrial fibrillation in the isolated sheep heart," *Circ.*, vol. 103, pp. 2631–2636, 2001.
[37] C. Morillo, G. Klein, D. Jones, and C. Guiraudon, "Chronic rapid atrial pacing. Structural, functional, and electrophysiological characteristics of a new model of sustained atrial fibrillation," *Circ.*, vol. 91, pp. 1588–1595, 1995.
[38] M. Haissaguerre, P. Jais, D. Shah, A. Takahashi, M. Hocini, G. Quiniou, S. Garrigue, A. L. Mouroux, P. L. Métayer, and J. Clémenty, "Spontaneous initiation of atrial fibrillation by ectopic beats originating in the pulmonary veins," *N. Eng. J. Med.*, vol. 339, pp. 659–666, 1998.

Martin Stridh (S'97–M'03) received the M.S. degree in electrical engineering from Lund University, Lund, Sweden in 1997 and the Ph.D. degree in signal processing in 2003.

He is presently Researcher with the Signal Processing Group. His research interests are statistical signal processing and time-frequency analysis with application to biomedical signals.

Leif Sörnmo (S'80–M'85) received the M.Sc. and D.Sc. degrees in electrical engineering from Lund University, Lund, Sweden, in 1978 and 1984, respectively.

He held a research position with the Department of Clinical Physiology, Lund University, from 1983 to 1995, where he worked on computer-based ECG analysis. Since 1990, he has been with the Signal Processing Group, Department of Electroscience, Lund University, where he now holds a position as a Professor in biomedical signal processing. He was on the editorial board of *Computers in Biomedical Research* from 1997 to 2000. His main research interests include statistical signal processing and modeling of biomedical signals. His current research projects include high-resolution ECG analysis, methods in ischemia monitoring, time-frequency analysis of atrial fibrillation, power efficient signal processing in pacemakers, and detection of otoacoustic emissions

Dr. Sörnmo has been an Associate Editor of the IEEE TRANSACTIONS ON BIOMEDICAL ENGINEERING since 2001.

Carl J. Meurling received the M.D. degree from Lund University, Lund, Sweden, in 1990, and the Ph.D. degree in cardiology, Lund University Hospital, in 2000.

He became a Specialist in General Internal Medicine in 1997 and a Specialist in Cardiology in 1999. His research is mainly concerned with noninvasive analysis of atrial fibrillatory electrophysiology.

S. Bertil Olsson is Professor of Cardiology at the Lund University Hospital, Lund, Sweden. His research interests include mechanisms and nonpharmocological treatment of different types of cardiac arrhythmias. Currently, he is leading several Ph.D. degree projects involving medical as well as technological aspects of atrial fibrillation.